Modeling differential transmission spectroscopy experiments in quantum dot optical amplifiers and saturable absorbers

Mattia Rossetti, Paolo Bardella, Ivo Montrosset*
Dipartimento di Elettronica, Politecnico di Torino,
C.so Duca Degli Abruzzi 24, 10129, Torino, Italy

ABSTRACT

We present a numerical model based on a time-domain travelling-wave approach to describe pulse propagation in InAs Quantum-Dot (QD) based Semiconductor Optical Amplifiers (SOA) and Saturable Absorbers (SA). The one-dimensional field propagation equation is solved in the time domain, in the slowly varying envelope approximation and it is coupled to a set of multi-population rate-equations modeling carrier dynamics in the QD layers in each longitudinal section of the waveguide. The optical response of the QD active medium is introduced in the field equation via a proper polarization term described as a set of infinite impulse response numerical filters. The inhomogeneous broadening of the density of states of the QD system induced by the QD size dispersion is properly taken into account. The influence of a static electric field on carrier dynamics in a reversely biased SA is described in the rate equations via bias dependent thermionic escape rates and tunneling processes. Absorption dynamics in a QD SA shows an initial ultrafast, bias independent recovery, followed by a slower recovery strongly dependent on the applied reverse bias. The QD SOA shows instead a dominant ultrafast gain recovery on a subpicosecond time scale at both QD Ground-States (GS) and first Excited-States (ES_1) wavelengths. Direct capture/escape processes between quantum well states and deeply confined QD states slightly influence the gain and absorption dynamics.

Keywords: Time-domain travelling-wave model, pump and probe experiments, quantum-dot, semiconductor optical amplifiers, saturable absorbers

1. INTRODUCTION

Quantum Dot (QD) Semiconductor Optical Amplifiers (SOA) have shown improved performances as components in high-speed optical signal processing applications if compared with their bulk or quantum-well (QW) counterparts, thanks to the ultrafast sub-picosecond gain recovery achievable in such devices. At the same time, QD based saturable absorbers (SA) have been successfully applied as mode-locking elements in solid state lasers and in integrated two-section passively mode-locked QD lasers, thanks to the fast absorption recovery obtained increasing the applied reverse bias. Experimental and theoretical studies of gain and absorption dynamics in such structures are therefore essential in order to optimize their performances. Differential Transmission Spectroscopy (DTS) has been shown to be a powerful technique to gain insights on the ultrafast dynamics of both QD SOAs and SAs.

DTS experiments in QD SOAs have shown gain recovery dominated by spectral hole burning non-linearity and characterized by a ultrafast time constant ranging form 100 fs to 300 fs[1]. Those measurements confirm the existence of efficient intraband carrier relaxation processes between QD confined states, mainly via Auger carrier-carrier scattering as theoretically predicted by Nielsen et al.[2]. Recently, many efforts have been done in order to understand the influence of capture processes from the two-dimensional QW/wetting layer (WL) states into the QD confined states. In past works[3], the slower refilling of QD excited states due to less efficient carrier capture processes, was supposed to represent an intrinsic limitation in the amplification of high repetition rate pulse trains. DTS measurements performed on InGaAs QD SOAs[4] showed however a gain recovery at wavelengths resonant with QD first excited states (ES_1) occurring on a time scale comparable with GS gain recovery. Moreover recent DTS experiments[5-6] have also shown no significant slow

*ivo.montrosset@polito.it; phone +39 011-090-4059; fax +39 011-090-4217; www.delen.polito.it

Semiconductor Lasers and Laser Dynamics IV, edited by Krassimir Panajotov, Marc Sciamanna, Angel A. Valle, Rainer Michalzik, Proc. of SPIE Vol. 7720, 77201I

down of the GS gain recovery after the injection of a high repetition rate optical pulse train. Gomis-Bresco et al. [6] explained this behaviour with the occurrence of extremely efficient direct capture processes from two dimensional QW states into the QD GSs and ESs, governed by characteristics time constants much smaller than the characteristic relaxation time from ES_1 to GS. Such a behaviour however is not consistent with capture time calculations provided by Nielsen[2] and Vallone[7] where direct capture processes were found to only weakly contribute to the overall carrier dynamics due to the large energy difference between initial and final states.

In section 3, we applied the time-domain travelling wave model described in section 2 to the analysis of gain dynamics in a SOA with active region consisting of 5 InAs QD layers embedded in InGaAs/GaAs quantum wells (DWELL) and emitting around 1.3 μm. Comparable gain recovery times for both GS and ES_1 gain have been found, consistently with experimental results shown by Borri[4]; moreover direct capture processes slightly contributes to the GS population dynamics. We have also found that the initial ultrafast recovery of the ES_1 gain is guaranteed by carrier relaxation from a second excited states (ES_2) that can be clearly identified from photo-luminescence experiments in such structures, as well as by efficient carrier capture from QW states to the QD ES_2 and ES_1.

In QD SA based on InAs DWELL layers, the influence of the applied junction voltage on the absorption dynamics has been experimentally studied via DTS experiments [8-9]. A bias independent fast absorption recovery of 1 ps has been reported[9]; on a longer time scale the absorption recovery is instead strongly influenced by the applied voltage: increasing the voltage, the characteristic time governing the absorption recovery is reduced from about 60 ps at 0V up to 1 ps at 10 V. This has been mainly attributed to the enhancement of thermionic emission due to a reduction of the activation energy and by additional escape contributions due to tunneling processes. In section 4, simulations of absorption recovery in reversely biased SA is reported for a SA with the same structure as the simulated SOA. A qualitative agreement with the experiments is achieved and details of the population dynamics in the QDs leading to the GS absorption dynamics are described.

2. TIME-DOMAIN TRAVELLING-WAVE MODEL FOR QD SOA AND SA

The amplitude of the guided mode travelling in the longitudinal direction (z) of a single mode ridge waveguide QD SOA or SA can be written as $\mathrm{E}(z,t) = E(z,t)e^{-jk_0 z}e^{+j\omega_0 t}$ and described by the following one dimensional wave equation in the slowly varying envelope approximation (SVEA):

$$\frac{1}{v_g}\frac{\partial E}{\partial t} + \frac{\partial E}{\partial z} = -j\frac{\omega_0}{2c\eta\varepsilon_0}\Gamma_{xy}P(z,t) - \frac{\alpha_i}{2}E(z,t); \tag{1}$$

where $E(z,t)$ is the slowly varying field envelope, v_g the group velocity, η is the effective refractive index of the guided mode, ε_0 is the vacuum electric permittivity, ω_0 is the reference frequency introduced in the SVEA and $k_0 = \omega_0\eta/c$ is the corresponding reference wave number. $P(z,t)$ is the slowly varying envelope of the polarization induced by the QD active medium, Γ_{xy} is the field confinement factor in a single DWELL layer and α_i are the intrinsic waveguide losses.

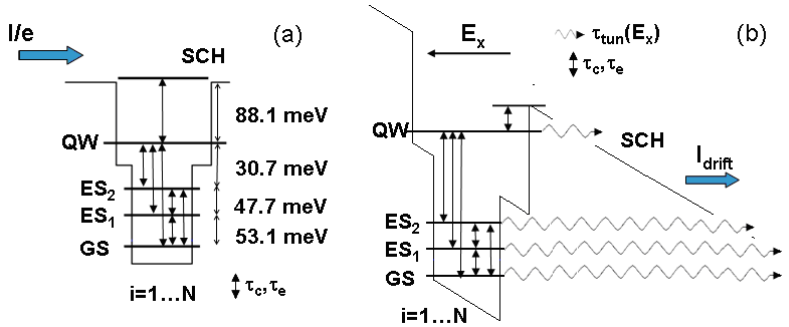

Figure 1. Schematics of the energy diagram of the QD layers for forward (a) and reversely biased (b) junction; arrows indicates possible capture, relaxation and escape paths between QD, QW, and barrier states (SCH). Symbols ∿▸ represents tunneling processes. In (a), numerical values refers to the QD group with highest existence probability.

The slowly varying field envelopes are normalized such that the forward travelling power is simply given by $|E(z,t)|^2$. The dynamics of $P(z,t)$ depends on the population dynamics in the QDs. In order to properly take into account the inhomogeneous broadening of the density of state of the whole QD system due to QD size dispersion, we subdivided the QD population in *N* groups according to their characteristic dimensions and energy diagram. QDs belonging to the same group are supposed to be identical, providing therefore equal contributions to the polarization $P(z,t)$. A qualitative scheme of the QD energy diagram is shown in figure 1. *N=11* QD groups have been considered throughout the paper. The population dynamics in the QDs belonging to the i[th] QD group (*i = 1...N*) and the corresponding dynamics of the microscopic QD polarizations can be described via a system of equations derived from a density matrix approach. These equations are coupled with rate equations describing carrier dynamics in the QW states and SCH states.
The complete set of equations in the case of current injection in the separate confinement heterostructure (SCH), reads as follows:

$$\begin{aligned}\frac{\partial \rho_{GS}^i}{\partial t} &= \frac{\mu_{ES1}}{\mu_{GS}}\tau_{cES1\to GS}^{-1}\rho_{ES1}^i\left(1-\rho_{GS}^i\right)-\tau_{eGS\to ES1}^{-1}\rho_{GS}^i\left(1-\rho_{ES1}^i\right)-\left(\tau_{eGS\to QW}^i\right)^{-1}\rho_{GS1}^i \\ &+\frac{\mu_{ES2}}{\mu_{GS}}\tau_{cES2\to GS}^{-1}\rho_{ES2}^i\left(1-\rho_{GS}^i\right)-\tau_{sGS}^{-1}\rho_{GS}^i+\tau_{eGS\to ES2}^{-1}\rho_{GS}^i\left(1-\rho_{ES2}^i\right)+\frac{h_w}{\mu_{GS}N_D}\tau_{cQW\to GS}^{-1}n_w\left(1-\rho_{GS}^i\right) \\ &-\tau_{AugGS}^{-1}\left(\rho_{GS}^i\right)^2-\frac{1}{\hbar}\frac{\Gamma_{xy}}{h_wW}\frac{1}{c\eta\varepsilon_0}\mathrm{Im}\left(d_{GS}^*p_{GS}^iE^*(z,t)\right),\end{aligned} \tag{2}$$

$$\begin{aligned}\frac{\partial \rho_{ES1}^i}{\partial t} &= -\tau_{cES1\to GS}^{-1}\rho_{ES1}^i\left(1-\rho_{GS}^i\right)+\frac{\mu_{GS}}{\mu_{ES1}}\tau_{eGS\to ES1}^{-1}\rho_{GS}^i\left(1-\rho_{ES1}^i\right)+\frac{\mu_{ES2}}{\mu_{ES1}}\tau_{cES2\to ES1}^{-1}\rho_{ES2}^i\left(1-\rho_{ES1}^i\right)-\tau_{AugES1}^{-1}\left(\rho_{ES1}^i\right)^2 \\ &-\tau_{sES1}^{-1}\rho_{ES1}^i-\tau_{eES1\to ES2}^{-1}\rho_{ES1}^i\left(1-\rho_{ES2}^i\right)+\frac{h_w}{\mu_{ES1}N_D}\tau_{cQW\to ES1}^{-1}n_w\left(1-\rho_{ES1}^i\right) \\ &-\left(\tau_{eES1\to QW}^i\right)^{-1}\rho_{ES1}^i-\frac{1}{\hbar}\frac{\Gamma_{xy}}{h_wW}\frac{1}{c\eta\varepsilon_0}\mathrm{Im}\left(d_{ES1}^*p_{ES1}^iE^*(z,t)\right),\end{aligned} \tag{3}$$

$$\begin{aligned}\frac{\partial \rho_{ES2}^i}{\partial t} &= \frac{h_w}{\mu_{ES2}N_D}\tau_{cQW\to ES2}^{-1}n_w\left(1-\rho_{ES2}^i\right)-\left(\tau_{eES2\to QW}^i\right)^{-1}\rho_{ES2}^i-\tau_{cES2\to ES1}^{-1}\rho_{ES2}^i\left(1-\rho_{ES1}^i\right)-\tau_{AugES2}^{-1}\left(\rho_{ES1}^i\right)^2 \\ &-\tau_{cES2\to GS}^{-1}\rho_{ES2}^i\left(1-\rho_{GS}^i\right)+\frac{\mu_{ES1}}{\mu_{ES2}}\tau_{eES1\to ES2}^{-1}\rho_{ES1}^i\left(1-\rho_{ES2}^i\right)+\frac{\mu_{GS}}{\mu_{ES2}}\tau_{eGS\to ES2}^{-1}\rho_{GS}^i\left(1-\rho_{ES2}^i\right)-\tau_{sES2}^{-1}\rho_{ES1}^i;\end{aligned} \tag{4}$$

$$\begin{aligned}\frac{\partial n_{QW}}{\partial t} &= \frac{h_{SCH}}{h_wN_w}\tau_{cSCH\to QW}^{-1}n_{SCH}-\tau_{eQW\to SCH}^{-1}n_{QW}-\sum_{i=1}^{N}\sum_{\substack{k=ES_2,\\ES_1,GS}}G_i\tau_{cQW\to k}^{-1}n_w\left(1-\rho_k^i\right) \\ &+\sum_{i=1}^{N}\sum_{\substack{k=ES_2,\\ES_1,GS}}G_i\frac{N_D\mu_k}{h_w}\left(\tau_{ek\to QW}^i\right)^{-1}\rho_k^i-\tau_{sQW}^{-1}n_{QW};\end{aligned} \tag{5}$$

$$\frac{\partial n_{SCH}}{\partial t} = \frac{J}{h_{SCH}e}-\tau_{cSCH\to QW}^{-1}n_{SCH}+\frac{h_wN_w}{h_{SCH}}\tau_{eQW\to SCH}^{-1}n_{QW}-\tau_{sSCH}^{-1}n_{SCH}; \tag{6}$$

$$\frac{\partial p_k^i}{\partial t} = \left\{j\left(\omega_k^i-\omega_0\right)+\Gamma\right\}p_k^i(t)+\frac{j}{\hbar}d_k\left(2\rho_k^i-1\right)E(z,t);\quad k=GS,ES_1 \tag{7}$$

$$P(z,t) = \frac{N_DN_w}{h_w}\sum_{i=1}^{N}\sum_{k=GS,ES}G_i\mu_kd_k^*p_k^i(z,t), \tag{8}$$

where ρ_k^i with $k=GS,ES_1,ES_2$ represent the occupation probabilities in the confined states of QDs belonging to the i^{th} QD group, p_k^i are the corresponding microscopic polarizations, μ_k is the degeneracy of the k[th] QD state and $\hbar\omega_k^i$ is the characteristic interband transition energy of state *k* in the i[th] QD group; n_{QW} and n_{SCH} represent the carrier densities in the

QW and in the SCH respectively. $\tau_{ck'\to k''}$ and $\tau_{ek'\to k''}$ are the characteristic times governing carrier energy relaxation processes and escape processes from state k' to state k''; escape times are related to the corresponding relaxation times via suitable expressions in order to guarantee the recovery of a quasi equilibrium energy distribution under no external perturbations[10]; moreover, in a forward biased SOA, $\tau_{cSCH\to QW}$ is considered as the sum of the characteristic time for carrier diffusion across the SCH region and the carrier capture time in the QW states. $\tau_{s\,k}$ accounts for monomolecular interband recombination and spontaneous emission from the state k whereas $\tau_{Aug\,k}$ describes Auger interband recombination from the state *k*. N_D is the QD surface density, N_w is the number of DWELL layers, h_{SCH} and h_w are the SCH and QW width respectively, *W* is the ridge width of the waveguide, and *J* is the current density injected in the SCH. Finally G_i represents the existence probability of the i[th] QD group. Throughout the paper a Gaussian distribution function is assumed so that G_i can be therefore written as $G_i = \exp\left(-4\ln 2\cdot\left(\hbar\omega_k^i - \hbar\omega_k^{(N+1)/2}\right)^2/\Delta E^2\right)/Z$ where ΔE is the Gaussian full width at half maximum (FWHM) and *Z* is a normalization constant such that $\sum_i G_i = 1\cdot$

Equations (2-6) describe the population dynamics in the QD layers in the excitonic approach whereas equation (7) determines the temporal evolution of the microscopic polarizations where Γ represents the dephasing rate for polarization determining the homogeneous linewidth of the corresponding interband transition and d_k is the dipole matrix element of the interband transition from state *k=GS,ES1*. In (7), the polarization dynamics associated to higher energy states has been neglected being significantly detuned in frequency with respect to the optical field coupled into the waveguide. The slowly varying envelope of the macroscopic polarization appearing in equation (1), can then be simply related to the microscopic QD polarizations via relation (8). Equations (1-8) represent therefore a complete set of equations to be solved in order to properly describe the pulse propagation in a QD SOA.

In order to model the population dynamics in a reversely biased SA however proper modifications to equations (2-6) must be introduced: the enhanced thermionic escape rates from the QD states to the QW states and from the QW to the SCH states, due to a linear barrier reduction induced by the applied electric field are modeled via modified expressions for the characteristic escape times $\tau^{Vi}_{ek'\to k''} = \tau^{i}_{ek'\to k''}\exp\left(e\left(V+V_{bi}\right)h_w/\left(h_{SCH}\,k_B T\right)\right)$ with $k' = GS, ES_1, ES_2 \to k'' = QW$ or $k' = QW \to k'' = SCH$, where *V* is the applied junction voltage, V_{bi} is the built-in potential of the junction, k_B is the Boltzmann constant and *T* is the device temperature. Additional escape paths due to tunneling processes from QD and QW states to the SCH sates are then introduced in equations (2-5). The tunneling rates can be estimated using the Wentzel–Kramer–Brillouin approximation for a triangular well[8]. Finally in the rate equation (6) for carriers in the SCH region, the current density *J* in the reversely biased SA represents a drift sweep-out contribution that can be written as $J = -e\mu_d n_{SCH}\,|V|/h_{SCH}$ where μ_d is the GaAs electron mobility.

To numerically solve equation (1) properly resolving both GS and ES_1 characteristic transition frequencies, we chose ω_0 as the central frequency between the GS and the ES_1 transitions of the QD group with the highest existence probability: $\omega_0 = \frac{1}{2}\left(\omega_{ES1}^{(N+1)/2} + \omega_{GS}^{(N+1)/2}\right)$; with this choice, the detuning between the injected optical pulse frequency and ω_0 remains small enough to guarantee the applicability of the SVEA.

Equation (1) must then be coupled to a proper boundary condition $E(0,t) = E_0(t)$ where $E_0(t)$ is the slowly varying amplitude of the external field coupled into the waveguide. Using equations (1), (7) and (8), one can obtain the following integro-differential equation:

$$\frac{1}{v_g}\frac{\partial E}{\partial t} + \frac{\partial E}{\partial z} = \frac{\omega_0}{2c\eta}\Gamma_{xy}\frac{N_D N_w}{h_w}\sum_{i=1}^{N}\sum_{k=GS,ES_1}\frac{G_i\mu_k}{\hbar\Gamma\varepsilon_0}|d_k|^2\left(u(t)\Gamma e^{-\Gamma t}e^{j\left(\omega_k^i-\omega_0\right)t}\right)\otimes\left(\left(2\rho_k^i(z,t)-1\right)E(z,t)\right) - \frac{\alpha_i}{2}E(z,t); \quad (9)$$

where $\otimes$ indicates a convolution integral and $u(t)$ is the unit step function. If one is interested in the dynamics on a time scale longer than the characteristic dephasing time for the polarizations $2\pi/\Gamma \approx 200\ fs$, one can treat the temporal changes of the populations ρ_k^i in adiabatic approximation leading to:

$$\frac{1}{v_g}\frac{\partial E}{\partial t}+\frac{\partial E}{\partial z}=\Gamma_{xy}\frac{\omega_0 N_D N_w}{2c\eta h_w}\sum_{i=1}^{N}\sum_{k=GS,ES}\frac{G_i\mu_k}{\hbar\Gamma\varepsilon_0}|d_k|^2\left(2\rho_k^i(z,t)-1\right)\cdot\left\{\left(u(t)\Gamma e^{-\Gamma t}e^{j(\omega_i^k-\omega_0)t}\right)\otimes E(z,t)\right\}-\frac{\alpha_i}{2}E(z,t) \tag{10}$$
$$=\sum_{i=1}^{N}\sum_{k=GS,ES}A_k^i\left(2\rho_k^i(z,t)-1\right)\cdot\left\{L_k^i(t)\otimes E(z,t)\right\}-\frac{\alpha_i}{2}E(z,t);$$

where we defined $A_k^i=\Gamma_{xy}\frac{\omega_0 N_D N_w}{2c\eta h_w}\frac{G_i\mu_k}{\hbar\Gamma\varepsilon_0}|d_k|^2$ and the convolution integral $L_k^i(t)\otimes E(z,t)=\left(u(t)\Gamma e^{-\Gamma t}e^{j(\omega_i^k-\omega_0)t}\right)\otimes E(z,t)$.

The convolution integral $L_k^i(z,t)\otimes E(z,t)$ simply represents the electric field envelope $E(z,t)$ filtered with a Lorentzian response function modeling the homogeneous-line broadening of the k^{th} interband transition in the ith QD groups. Within the adiabatic approximation introduced in equation (10), it is therefore possible to define time varying net modal gain and refractive index spectra induced by the QDs as follows:

$$g(\omega,z,t)=2\sum_{i=1}^{N}\sum_{k=GS,ES_1}A_k^i\left(2\rho_k^i(z,t)-1\right)\mathrm{Re}\left\{\tilde{L}_k^i(\omega)\right\}-\alpha_i; \tag{11}$$

$$\Delta n(\omega,z,t)=\frac{c}{\omega_0}\sum_{i=1}^{N}\sum_{k=GS,ES_1}A_k^i\left(2\rho_k^i(z,t)-1\right)\mathrm{Im}\left\{\tilde{L}_k^i(\omega)\right\}; \tag{12}$$

where $\tilde{L}_k^i(\omega)=F\left\{L_k^i(t)e^{j\omega_0 t}\right\}=\frac{1}{1+j\left(\omega-\omega_k^i\right)/\Gamma}$ is the Lorentzian function representing the homogeneous line broadening of the interband transition from state k of the ith QD group, where $F\{...\}$ denotes the Fourier transform.

The field propagation equation (10) can be solved, together with equations (2-6) describing the population dynamics in the DWELL layers, using a finite-difference approach where the convolution product appearing in the right hand side of the equation (10) is simply modeled as the superposition of infinite impulse response (IIR) numerical filters with Lorentzian response function. Being Δz the unit step of a longitudinal discretization of the waveguide and defining $\Omega=\omega-\omega_0$, the solution of (10) in frequency domain can be approximated as follows

$$\tilde{E}(\Omega,z+\Delta z)\cong\exp\left\{-j\frac{\Omega}{v_g}\Delta z-\frac{\alpha_i}{2}\Delta z+\Delta z\sum_{i=1}^{N}\sum_{k=GS,ES}A_k^i\left(2\tilde{\rho}_k^i(z,\Omega)-1\right)\otimes\tilde{L}_k^i(\Omega)\cdot\right\}\tilde{E}(z,\Omega)\cong$$
$$\cong\exp\left(-j\frac{\Omega}{v_g}\Delta z\right)\cdot\left\{\tilde{E}(z,\Omega)-\frac{\alpha_i}{2}\tilde{E}(z,\Omega)\Delta z+\sum_{i=1}^{N}\sum_{k=GS,ES}A_k^i\left(2\tilde{\rho}_k^i(z,\Omega)-1\right)\otimes\left(\tilde{L}_k^i(\Omega)\cdot\tilde{E}(z,\Omega)\right)\Delta z\right\}; \tag{13}$$

where symbol $\tilde{X}$ denotes the Fourier transform of X with respect to time. Coming back in time domain one obtains the following time stepped solution for the propagation equation (10):

$$E(t+\Delta t,z+\Delta z)\cong E(t,z)+\sum_{i=1}^{N}\sum_{k=GS,ES}A_k^i\left(2\rho_k^i(z,t)-1\right)\cdot\left\{L_k^i(t)\otimes E(z,t)\right\}\Delta z-\frac{\alpha_i}{2}E^{\pm}(t,z)\Delta z; \tag{14}$$

where $\Delta t=\Delta z/v_g$ represents the unit time step.

The convolution product $I_k^i(z,t)=L_k^i(t)\otimes E(z,t)=\Gamma\int_{-\infty}^{t}e^{j(\omega_k^i-\omega_0)(t-\tau)}e^{-\Gamma(t-\tau)}E(\tau,z)d\tau$ can finally be simply computed as a IIR Lorentzian filter, using the following recursive relation:

$$I_k^i(t,z)=e^{j(\omega_k^i-\omega_0)\Delta t}e^{-\Gamma\Delta t}I_k^i(t-\Delta t,z)+\frac{1}{2}\Gamma\Delta t\left[E(t,z)+e^{j(\omega_k^i-\omega_0)\Delta t}e^{-\Gamma\Delta t}E(t-\Delta t,z)\right] \tag{15}$$

Equations (14) and (15) represent therefore a complete time-stepped solution of the propagation equation (10). Equation (14) however contains the dependence on the dynamics of carrier occupation probabilities $\rho_k^i(z,t)$. The population

dynamics is therefore obtained by solving the set of equations (2-6) in each slice $[z-\Delta z/2, z+\Delta z/2]$ of the longitudinally discretized waveguide where the microscopic polarizations appearing in equation (2) and (3) and determining the stimulated emission/absorption rate from the state k can be written as

$$p_k^i(t,z) = j\frac{d_k}{\hbar\Gamma}\left(2\rho_k^i(t,z)-1\right)I_k^i(t,z) \tag{16}$$

In this way pulse propagation in QD SOA or SA can be fully described and the temporal dynamics of QD gain and absorption spectra as well as the refractive index changes induced by the pump pulse can be monitored in each longitudinal section of the waveguide via expressions (11) and (12).

In DTS experiments, the gain changes induced by the pump pulse are measured by monitoring the transmission of weak probe pulses with variable delay times relative to the pump. The probe pulse energy is assumed to be small enough such that the gain dynamics is not significantly perturbed. Within this assumption, considering a reference framework moving with the probe pulse, the single pass gain experienced by the weak probe pulse can be simply approximated as:

$$G(\omega,\tau) = \exp\left\{\int_0^L g(\omega,z,\tau+z/v_g)dz\right\} \tag{17}$$

where L is the waveguide length, g is the net modal gain calculated via expression (11) and τ is the time delay between pump and probe pulses. In the following sections, gain/absorption dynamics induced by the propagation of a pump pulse in a QD SOA and SA are studied as a function of the applied bias conditions. In the results presented below, we always considered probe pulses with the same frequency as the frequency of the pump pulse, ω_p. Neglecting spectral artifacts related to the finite bandwidth of the probe pulse, the changes in the probe single pass gain induced by the pump pulse have been simply written as $\Delta G(\omega_p,\tau) = G(\omega_p,\tau) - G_0(\omega_p)[dB]$ where $G_0(\omega_p)$ is the single pass gain experienced by the probe pulse in absence of the pump induced perturbation (expressed in dB).

3. GAIN RECOVERY IN A QD SEMICONDUCTOR OPTICAL AMPLIFIER

We consider a 500 μm long QD SOA with 5 μm ridge width and active region consisting of 5 InAs/$In_{0.15}Ga_{0.85}As$ DWELL layers emitting around 1.3 μm. The main parameters appearing in equations (1-17) and used in the simulations are the following: $N=11$, $\Gamma_{xy}=1.274\%$, $\eta=3.3445$, $\alpha_i=1.5cm^{-1}$, $\mu_{GS}=2$, $\mu_{ES1}=4$, $\mu_{ES2}=6$, $\tau_{cES\,2\to ES\,1}=0.27\ ps$, $\tau_{cQW\to k}=\{0.5,0.6,0.8\}$ ps for $k=\{ES_2,ES_1,GS\}$, $\tau_{cES\,1\to GS}=0.33\ ps$, $\tau_{cES\,2\to GS}=0.7\ ps$, $\tau_{cSCH\to QW}=245+0.2\,ps$, $N_D=3\cdot10^{10}\ cm^2$, $\tau_{sk}=\{200,200,2.7\cdot10^3,2\cdot10^3,2\cdot10^3\}ps$ for $k=\{SCH,QW,ES_2,ES_1,GS\}$, $\Delta E=34\ meV$, $\hbar\Gamma=12\ meV$, $\hbar\omega_k^{(N+1)/2}=\{1.0543,\ 0.9879\}\ eV$ for $k=\{ES_1,GS\}$. Finally, the energy diagram of confined states in the QD layers is shown in figure 1a.

In all the figures below, the following notation is used: continuous lines represent results obtained when all the scattering processes depicted in figure 1a are taken into account, dotted lines show instead data obtained neglecting direct capture and escape process between the QW states and the deeply confined QD states ES_1 and GS.

Figure 2a shows the net modal gain spectra for various values of injected current computed in absence of external optical excitation. At a fixed current, net modal gain spectra are slightly larger when direct capture processes are taken into account. This can be justified by the reduced gain saturation induced by spontaneous emission recombination in the QD states.

To study the gain dynamics in the QD SOA, we then consider an un-chirped Gaussian pump pulse with 150 fs width, 1.28 pJ energy and central frequency resonant with either GS ($\hbar\omega_p=0.9879\ eV$) or ES_1 ($\hbar\omega_p=1.0573\ eV$) transitions.

The pump induced changes in the single pass gain experienced by the probe pulse as a function of the delay time relative to the pump pulse, $\Delta G(\omega_p,\tau)$, are shown in figures 2b and 2c for ω_p resonant with GS and ES_1 respectively. In the gain regime, the pump pulse strongly depletes carrier populations in the QD states resonant with the pulse frequency, leading to a significant gain compression.

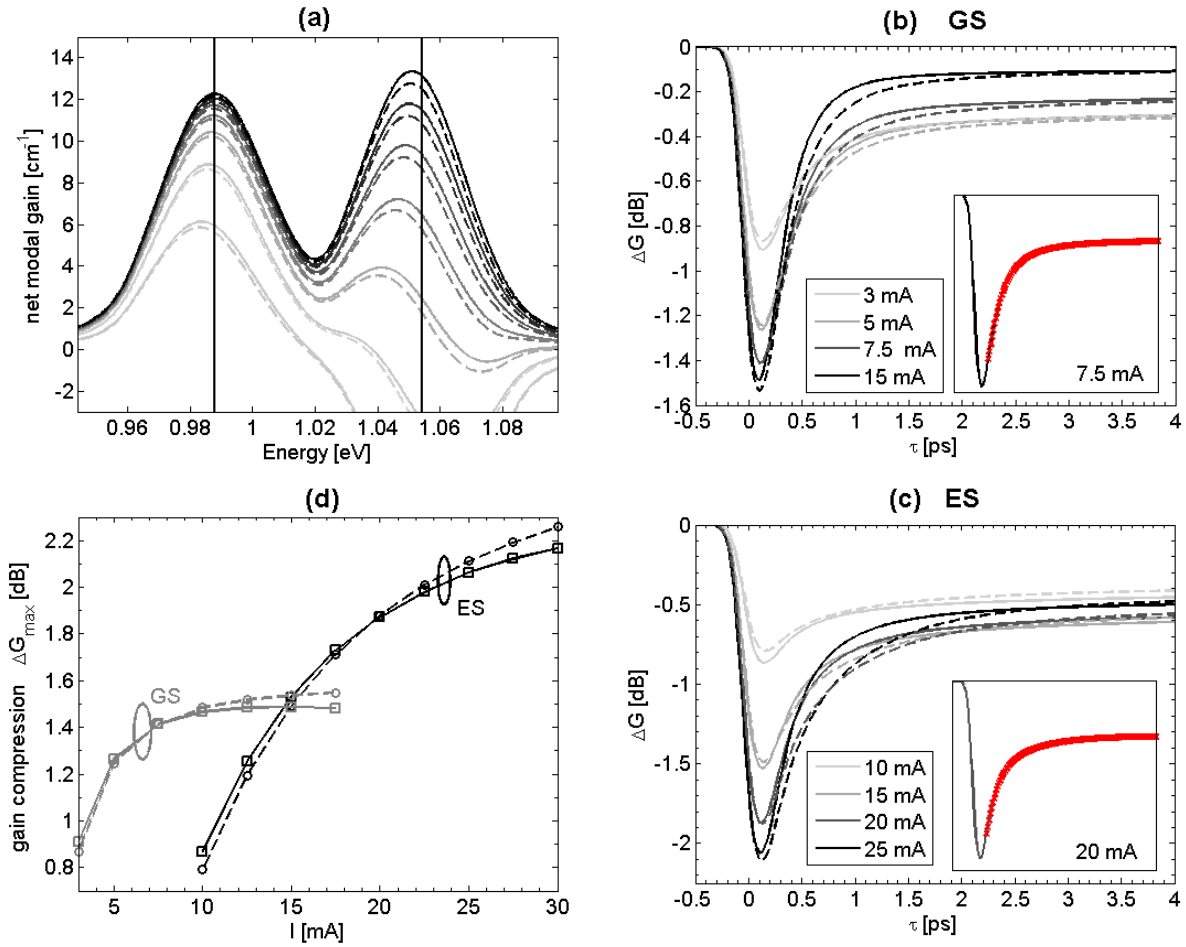

Figure 2. (a) Net modal gain spectra for current I=3,5, 7.5, 10, 12.5, 15, 17.5 mA; vertical lines show the frequency of pump pulses resonant with GS and ES_1 transitions, respectively; (b) gain dynamics induced by a pump pulse resonant with the GS transitions ($\hbar\omega_p = 0.9879$ eV) for I = 3, 5, 7.5, 15 mA, inset: fitting of the gain dynamics at 7.5 mA with a double exponential response function; (c) gain dynamics induced by a pump pulse resonant with the ES_1 transitions ($\hbar\omega_p = 1.0543$ eV) for I = 10, 15, 20 , 25 mA; inset: fitting of gain dynamics at 20 mA as in (b); (d) Maximum gain compression versus current. Continuous and dashed lines represent results obtained considering and neglecting direct capture/escape processes, respectively.

The maximum gain compression $\Delta G|_{max}$ induced by the pump pulse is shown in figure 2d as a function of the injected current. $\Delta G|_{max}$ monotonically increases with current following the increase in the steady state net modal gain (figure 1a). Direct capture processes only slightly influences this quantity: at low currents $\Delta G|_{max}$ is faintly larger when capture processes are considered mainly due to the larger initial steady state gain at both GS and ES_1 wavelengths; at higher currents, the more efficient refilling of QD states due to direct capture processes causes instead a reduction of the total gain compression with respect to the case with no direct capture processes.

At both GS and ES_1 wavelengths, gain dynamics then shows a dominant ultrafast recovery completed in a picosecond time scale; subsequent long-lasting changes occurring on a time scale of hundreds of picoseconds can then be identified, leading to a clear offset in the gain curve within the investigated time interval. As expected, direct capture processes tend to speed up the gain recovery at both GS and ES_1 wavelengths whereas the long-lasting changes determining the offset in the gain recovery curve remain practically unchanged. Such slow dynamics cannot therefore be attributed to slow carrier capture in the QD states but it is mainly due to changes in the total carrier density in the active region, limited by carrier diffusion across the SCH ($\tau_{cSCH \to QW}$).

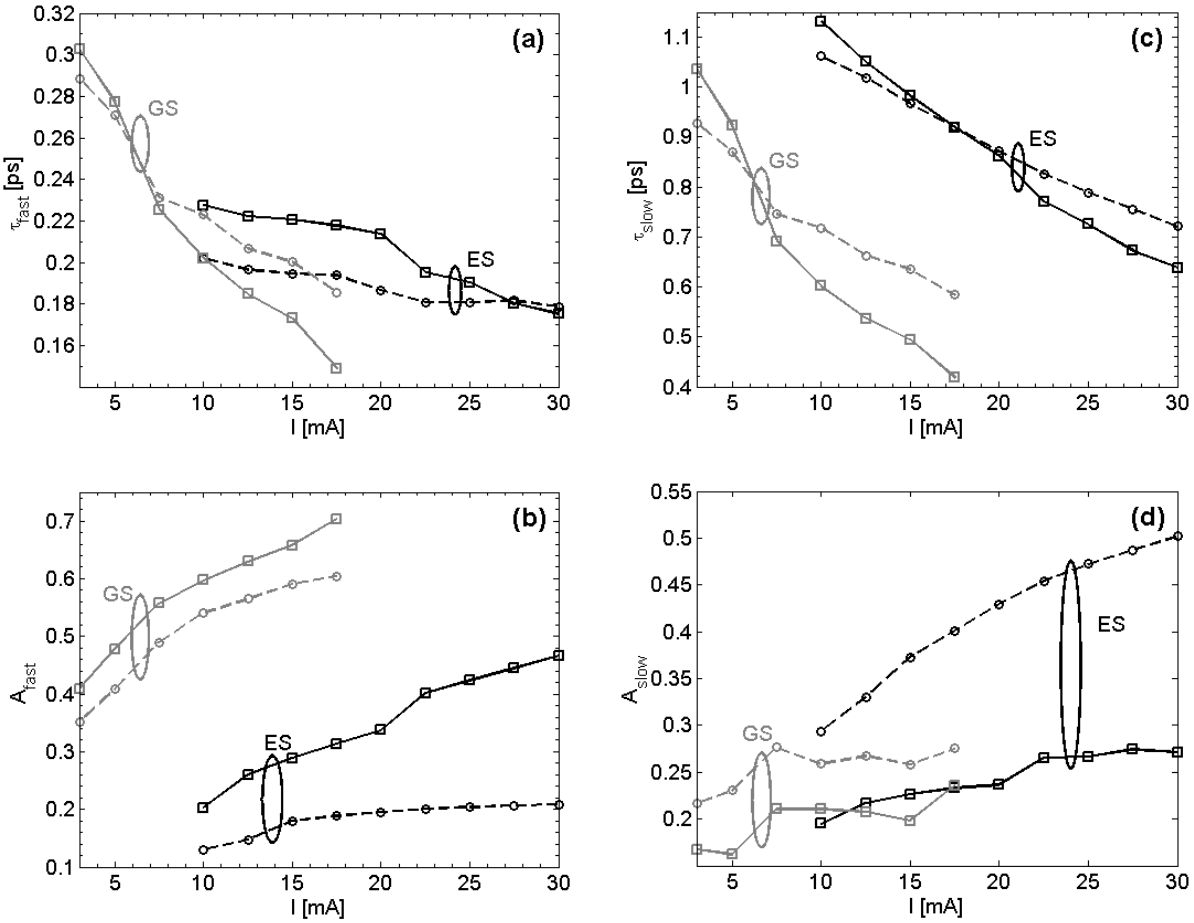

Figure 3. Characteristics time constants τ_{fast}, τ_{slow} and corresponding amplitudes relative to the total gain compression A_{fast} and A_{slow}, obtained by fitting the gain dynamics with a double exponential function. Continuous lines with square markers are obtained considering direct capture processes, dashed lines with round markers show results of simulations where such processes have been neglected. Black and grey curves represent data for ES_1 and GS gain dynamics, respectively.

According to the experimental results shown by Borri[4], the obtained gain recovery can be well fitted with a double exponential function $\Delta G(\tau) = \Delta G_{\max}\left[A_0 + A_{fast}\exp\left(-\tau/\tau_{fast}\right) + A_{slow}\exp\left(-\tau/\tau_{slow}\right)\right]$ where τ_{fast} and τ_{slow} are the characteristic time constants, A_{fast} and A_{slow} are the corresponding amplitudes relative to the total gain compression and A_0 is an offset accounting for the slow dynamics discussed above. The fitting has been performed using the Prony method and two examples of fitted gain dynamics are shown in the insets of figures 2b-c.

In figure 3a-d the obtained time constants and their corresponding amplitudes are plotted as a function of the applied current. GS gain recovery is characterized by an ultrafast time constant τ_{fast} in the range between 300 and 150 fs, and by a slower recovery time τ_{slow} ranging from 1 ps to 400 fs. Both time constants decrease significantly with the applied current whereas their amplitudes tend to increase. ES_1 gain recovery shows values of τ_{fast} comparable with GS gain recovery consistently with experimental findings of an initial ultrafast gain recovery also at the ES wavelengths. The corresponding amplitude A_{fast} characterizing the ES_1 gain dynamics is however significantly reduced with respect to the one describing the GS gain dynamics (figure 3b) and the ES_1 gain recovery tends to be dominated by a longer time

constant τ_{slow} with a value significantly larger than the one found for the GS dynamics (figure 3c). The described picture is in good agreement with published DTS experiments[4].

The existence of an ultrafast ES_1 gain recovery time constants τ_{fast} comparable with the GS one is attributed here to the presence of a higher energy QD excited state (ES_2) with larger degeneracy acting as a reservoir and allowing for an efficient carrier relaxation into the QD ES_1, as well as to efficient capture processes from the QW states into the higher energy QD states, ES_2 and ES_1.

Introducing direct capture processes in the simulations, only small changes in the time constants τ_{fast} and τ_{slow} are obtained. Direct capture processes lead however to a significant increase in the amplitude of the faster time constant A_{fast} to the detriment of the magnitude of the amplitude A_{slow}.

4. ABSORPTION RECOVERY IN A QD SATURABLE ABSORBER

In this section we present simulations of the same device described in the previous section, acting now as a SA.

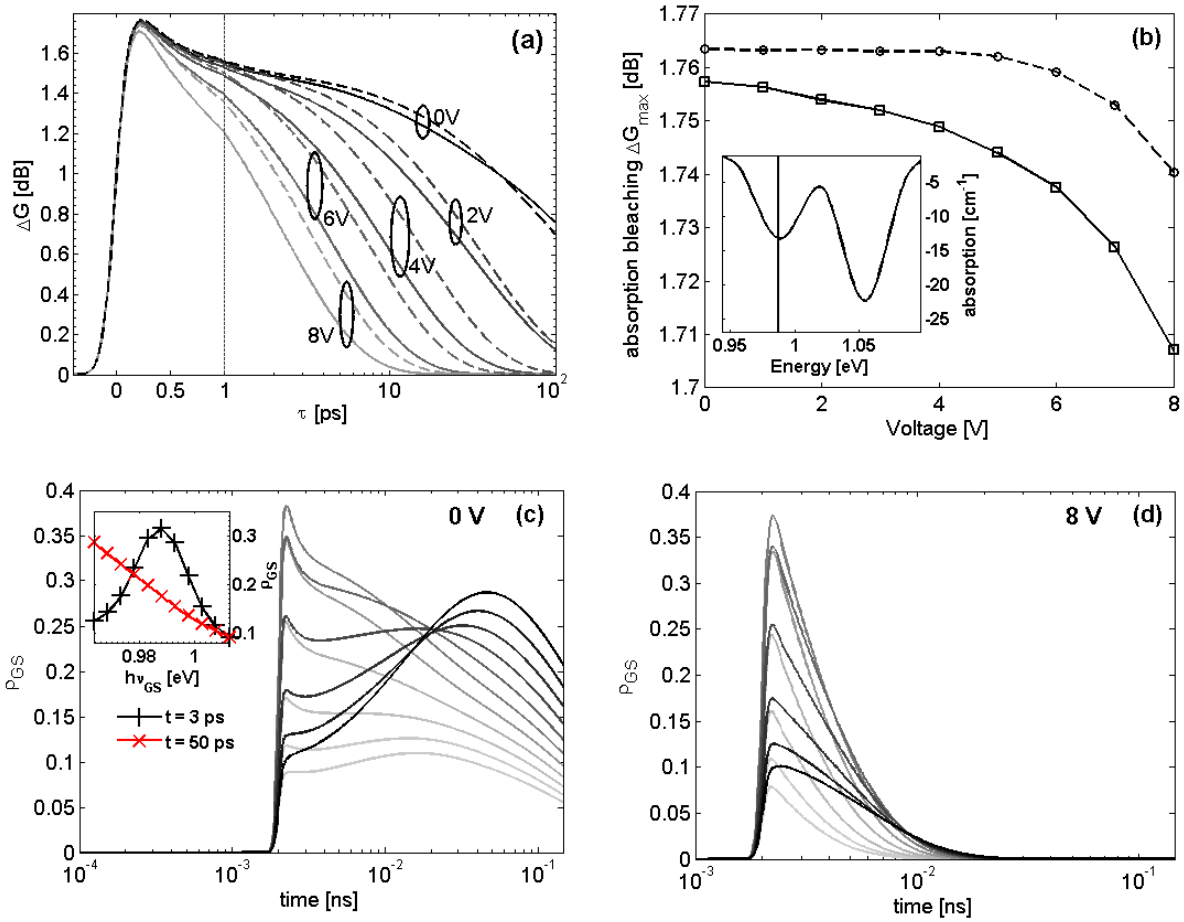

Figure 4. (a) Absorption dynamics for voltage ranging from 0-8 V; time axis is shown in linear scale up to 1 ps; from 1 ps to 100 ps, time axis is displayed in logarithmic scale for clarity; (b) maximum absorption bleaching induced by the pump pulse versus the applied voltage; inset shows net modal absorption spectra of the unperturbed SA; (c-d) dynamics of the GS occupation probabilities in the 11 QD groups from group 1 with $\hbar\omega_{GS}^{1} = 0.9633$ eV (black curve) to group 11 with $\hbar\omega_{GS}^{11} = 1.0124$ eV (light grey), at z=250 μm, for 0V and 8V respectively. Inset shows the occupation probability versus GS interband transition energies for t=3 ps and t=50 ps at 0V.

We consider a voltage applied to the p-i-n junction ranging from 0 V (short circuit) to 8 V and a pump pulse resonant with the GS transitions. The obtained absorption dynamics is shown in figure 4a for different bias values. The absorption of the strong pump pulse causes the generation of carriers in the QD GSs leading to a reduction of the absorption.

The subsequent absorption recovery can be well fitted using a double exponential function as for the SOA gain dynamics. At low applied voltages, a ultrafast absorption recovery time τ_{fast} ranging from 400 to 300 fs is obtained as shown in figure 5a; this dynamics is associated to the efficient excitation of the photo-generated GS carriers to higher energy states ES_1 and ES_2. The amplitude of this ultrafast recovery A_{fast} is however significantly smaller than the one of the ultrafast component in the SOA gain recovery and decreases further when the applied voltage is increased. The absorption recovery is instead dominated by a slower time constant τ_{slow}, strongly dependent on the applied reverse bias, decreasing from 35.2 ps at 0V up to 2.4 ps at 8V as shown in figure 5a. The decrease of the absorption recovery time with the applied voltage also leads to a reduction of the maximum absorption bleaching induced in the SA by the strong pump pulse as shown in figure 4b.

In order to better understand the physical mechanisms leading to the absorption recovery, the dynamics of the occupation probabilities in the GSs of different QD groups in z=250 μm, for an applied bias of 0V and 8V is shown in figure 4c and 4d respectively. The absorption of the strong pump pulse generates carriers in the GSs belonging to the various QD groups, according to the shape of the pulse spectrum. The initial ultrafast excitation of carriers from the GS to higher energy QD states is then clearly visible in the case of a 0V applied bias. For this voltage, on a time scale of several picoseconds, thermionic escape from the QD states towards the QW states allows the thermalization of carriers among the various QD groups; the occupation probabilities of groups with the lowest GS energy increase therefore with time, guaranteeing the recovery of a quasi-equilibrium energy distribution of carriers in the whole QD population (figure 4c and inset). The absorption recovery is then completed thanks to non radiative recombination and spontaneous emission processes occurring on a time scale of several hundreds of picoseconds.

Increasing the applied voltage, thermionic escape towards the QW states is significantly enhanced due to the reduction of the barrier energy induced by the applied electric field; for reverse bias larger then 4V however tunneling processes from the QD states towards the three dimensional SCH states become the dominant contribution to the absorption recovery. Looking at the GS occupation probability dynamics for 8V reverse bias (figure 4d), carrier thermalization between different QD groups is prevented by the fast sweep out of carriers from the GSs due to efficient tunneling processes towards the SCH states.

Direct escape processes between the deeply confined QD states and the QW states reduces the characteristic recovery time τ_{slow} whereas its corresponding amplitude remains practically unchanged: from 0 to 2 V, absorption recovery is almost unaffected by direct escape processes, a further increase in the voltage however significantly enhances direct thermionic emission from deeply confined QD states and QW states due to the reduction in the barrier energy with the applied electric field.

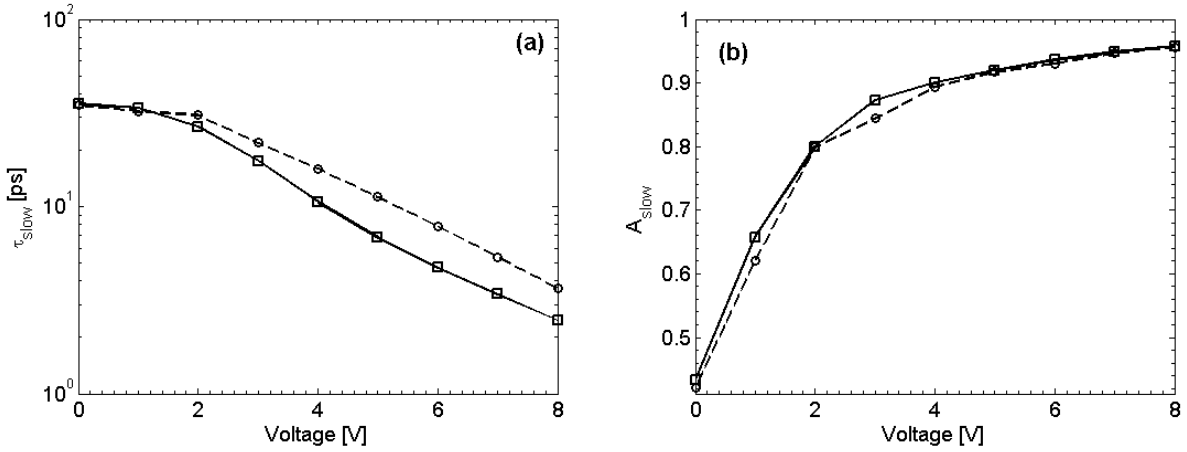

Figure 5. (a) Characteristics time constant τ_{slow} and corresponding amplitude relative to the total absorption bleaching A_{slow} versus the applied voltage, obtained by fitting the gain dynamics with a double exponential function.

5. CONCLUSIONS

We presented a time-domain travelling wave model for the analysis of pulse propagation in both QD SOAs and SAs. The model was applied to the study of gain/absorption dynamics in QD SOA and SA: the main physical mechanisms leading to fast gain/absorption recovery rates were described and the role of direct capture/escape processes between QW states and deeply confined QD states were highlighted. An agreement with published DTS experiments was obtained.

In future works, the numerical model will be extended to the analysis of passively mode locked (ML) two-section QD lasers. From this point of view, the work presented above represents an essential preliminary analysis of the QD gain and absorption dynamics governing the pulse generation in integrated QD ML lasers.

This work has received funding from the European Community's Seventh Framework Programme (FP7/2007-2013) under grant agreement n° 224338 (FAST-DOT project).

REFERENCES

[1] Borri, P., Langbein, W., Hvam, J. M., Heinrichsdorff, F., Mao, M.-H., Bimberg, D., "Spectral hole-burning and carrier-heating dynamics in InGaAs quantum-dot amplifiers", IEEE J. Select. Topics Quantum Elect. 6(3), 544-551 (2000).

[2] Nielsen, T. R., Gartner, P. and Jahnke, F., "Many-body theory of carrier capture and relaxation in semiconductor quantum-dot lasers", Phys. Rev. B 69, 235314 (2004).

[3] Berg, T. W., Bischoff, S., Magnusdottir, I., Mørk, J., "Ultrafast gain recovery and modulation limitations in self-assembled quantum-dot devices", IEEE Photon. Technol. Lett. 13(6), 541-543 (2001).

[4] Borri, P., Schneider, S., Langbein, W. and Bimberg, D., "Ultrafast carrier dynamics in InGaAs quantum dot materials and devices", J. Opt. A 8, S33-S46 (2006).

[5] Borri, P., Arekar, T., Cesari, V., Rossetti, M., Fiore, A., Langbein, W., "Ultrafast pulse-pair amplification in InGaAs quantum-dot amplifiers", Conference on Lasers and Electro-Optics CLEO/Europe, June 14-19, (2009).

[6] Gomis-Bresco, J., Dommers, S., Temnov, V. V., Woggon, U., Martinez-Pastor, J., Laemmlin, M., Bimberg, D., "InGaAs Quantum Dots Coupled to a Reservoir of Nonequilibrium Free Carriers", IEEE J. Quantum Electron. 45(9), 1121-1128 (2009).

[7] Vallone, M., "Many-body formulation of carriers capture time in Quantum Dots applicable to device simulation codes", J. Appl. Phys. 107, 053718 (2010).

[8] Malins, D.B., Gomez-Iglesias, A., White, S.J., Sibbett, W., Miller, A. and Rafailov, E.U., "Ultrafast electroabsorption dynamics in an InAs quantum dot saturable absorber at 1.3μm", App.Phys.Lett. 89, 171111 (2006).

[9] Thompson, M. G., Marinelli, C., Chu, Y., Sellin, R. L., Penty, R. V., White, I. H., Van Der Poel, M., Bikedal, D., Hvam, J., Ustinov, V. M. , Lammlin, M. and Bimberg, D., "Properties of InGaAs quantum dot saturable absorbers in monolithic mode-locked lasers", Conference Digest of the 19th International Semiconductor Laser Conference, Sept. 25, (2004).

[10] Gioannini, M. and Montrosset, I., "Numerical analysis of the frequency chirp in quantum-dot semiconductor lasers," IEEE J. Quantum Electron. 43(10), 941–949 (2007).